Online Appendix
Selective Visibility and Coordination Loss in Matching Markets:
An Evolutionary Model of Aspirational Search

Anonymous manuscript

1 Proofs of the general analytical results

1.1 Proof of Proposition 1: truthful selection raises perceived position

Let $a = sr$ and write $u(s, r) = \tilde{u}(a)$ with $\tilde{u}'(a) \geq 0$. Under the selective distribution,

$$\mathbb{E}_{G_S}[u] = \frac{\mathbb{E}_{G_0}[u(a)e^{\eta a}]}{\mathbb{E}_{G_0}[e^{\eta a}]}.$$

Therefore

$$\mathbb{E}_{G_S}[u] - \mathbb{E}_{G_0}[u] = \frac{\mathrm{Cov}_{G_0}(u(a), e^{\eta a})}{\mathbb{E}_{G_0}[e^{\eta a}]}.$$

Both $u(a)$ and $e^{\eta a}$ are nondecreasing in a. Their covariance is nonnegative by the standard covariance inequality for comonotone functions and is strictly positive when G_0 is nondegenerate in a and u is strictly increasing on a set of positive measure. Because

$$Q(z) = \bar{q}_0 + (1 - z)\mathbb{E}_{G_0}[u] + z\mathbb{E}_{G_S}[u],$$

we obtain

$$Q_z = \mathbb{E}_{G_S}[u] - \mathbb{E}_{G_0}[u] \equiv \chi > 0.$$

All realizations remain genuine; the result follows solely from differential sampling weights.

1.2 Proof of Proposition 2: existence and calibration

Fix $z = 0$ and suppress the cross-side channel. Define $f_0(x) = F(Q_0, x, \bar{y})$. By assumption, f_0 is continuous, $f_0(0) > 0 > f_0(1)$, and $f_0'(x) = F_x < 0$. The intermediate value theorem gives at least one root $x_0^* \in (0, 1)$, while strict monotonicity gives uniqueness. The one-dimensional replicator equation is

$$\dot{x} = x(1 - x)f_0(x).$$

For $x < x_0^*$, strict monotonicity implies $f_0(x) > 0$ and therefore $\dot{x} > 0$. For $x > x_0^*$, $f_0(x) < 0$ and therefore $\dot{x} < 0$. Every interior trajectory consequently moves toward x_0^*, which is globally asymptotically stable on $(0, 1)$.

1.3 Proof of Proposition 3: visibility-to-search comparative static

An interior M1 equilibrium satisfies

$$F(Q(z, 0), x_1^*(z), \bar{y}) = 0.$$

Differentiate with respect to z:

$$F_q Q_z + F_x \frac{\mathrm{d}x_1^*}{\mathrm{d}z} = 0.$$

Since $F_x \neq 0$, the implicit-function theorem gives

$$\frac{\mathrm{d}x_1^*}{\mathrm{d}z} = -\frac{F_q Q_z}{F_x} > 0.$$

1.4 Proof of Theorem 1: bilateral propagation, uniqueness, and local stability

An interior M2 equilibrium satisfies

$$F(Q(z,\tau),x^*,y^*)=0, \qquad H(x^*,y^*)=0.$$

Differentiating with respect to z yields

$$\begin{pmatrix} F_x & F_y \\ H_x & H_y \end{pmatrix}\begin{pmatrix} x_z^* \\ y_z^* \end{pmatrix} = -\begin{pmatrix} F_q Q_z \\ 0 \end{pmatrix}.$$

Let $\Delta = F_x H_y - F_y H_x$. The sign restrictions imply $\Delta > 0$. Inversion gives

$$x_z^* = -\frac{H_y F_q Q_z}{\Delta} > 0, \qquad y_z^* = \frac{H_x F_q Q_z}{\Delta} < 0.$$

For uniqueness, solve $F=0$ locally as $x=\varphi(y)$ and $H=0$ as $x=\psi(y)$. The implicit-function theorem gives

$$\varphi'(y) = -\frac{F_y}{F_x} > 0, \qquad \psi'(y) = -\frac{H_y}{H_x} < 0.$$

Hence an increasing and a decreasing nullcline can intersect at most once in the interior.

At the interior equilibrium the replicator Jacobian is

$$J_2 = \begin{pmatrix} XF_x & XF_y \\ YH_x & YH_y \end{pmatrix}, \qquad X = x^*(1-x^*) > 0, \quad Y = y^*(1-y^*) > 0.$$

Its trace is $XF_x + YH_y < 0$, and its determinant is

$$XY(F_xH_y - F_yH_x) = XY\Delta > 0.$$

Negative trace and positive determinant imply local asymptotic stability.

1.5 Proof of Proposition 4: global convergence under inward boundary conditions

Use the Dulac function

$$B(x,y) = \frac{1}{x(1-x)y(1-y)}.$$

For the M2 vector field,

$$B\dot{x} = \frac{F(Q,x,y)}{y(1-y)}, \qquad B\dot{y} = \frac{H(x,y)}{x(1-x)}.$$

Hence

$$\frac{\partial(B\dot{x})}{\partial x} + \frac{\partial(B\dot{y})}{\partial y} = \frac{F_x}{y(1-y)} + \frac{H_y}{x(1-x)} < 0$$

throughout $(0,1)^2$. By the Bendixson–Dulac criterion, no periodic orbit lies in the interior. The uniform boundary sign conditions point interior trajectories away from every edge, so no interior trajectory has an omega-limit set on the boundary. Theorem 1 gives a unique interior equilibrium. Poincaré–Bendixson then implies that every interior trajectory converges to that equilibrium.

1.6 Proof of Proposition 5: visibility-induced coordination loss

Along the equilibrium path,

$$\frac{\mathrm{d}M^*}{\mathrm{d}z} = M_x x_z^* + M_y y_z^*.$$

The maintained durable-matching restrictions give $M_x < 0$ and $M_y > 0$. Theorem 1 gives $x_z^* > 0$ and $y_z^* < 0$. Both terms are strictly negative, so $\mathrm{d}M^*/\mathrm{d}z < 0$.

1.7 Proof of Proposition 6: representativeness restoration

From

$$Q(z, \tau) = Q_0 + (1 - \tau)\chi z$$

we have $Q_\tau = -\chi z < 0$ for $z > 0$. Differentiating the M2 equilibrium system with respect to τ gives

$$x^*_\tau = -\frac{H_y F_q Q_\tau}{\Delta} < 0, \qquad y^*_\tau = \frac{H_x F_q Q_\tau}{\Delta} > 0.$$

Since $M_x < 0$ and $M_y > 0$,

$$M^*_\tau = M_x x^*_\tau + M_y y^*_\tau > 0.$$

1.8 Proof of Proposition 7: interior existence in M3

Under the uniform boundary-crossing conditions and strict own-state monotonicity, for each (y, z) there is a unique $x = R_F(y, z) \in (0, 1)$ solving $F(Q(z, \tau), x, y) = 0$. Likewise, for each x there is a unique $y = R_H(x) \in (0, 1)$ solving $H(x, y) = 0$, and for each (x, y) there is a unique $z = R_P(x, y) \in (0, 1)$ solving $P(x, y, z) = 0$. Continuity of F, H, and P, together with the strict own-state derivatives, implies continuity of the root mappings. Define

$$T(x, y, z) = \big(R_F(y, z), R_H(x), R_P(x, y)\big).$$

This is a continuous self-map of the compact convex cube $[0, 1]^3$, with image in $(0, 1)^3$. Brouwer's fixed-point theorem gives a fixed point (x^*, y^*, z^*), which is an interior equilibrium of the three-population system.

1.9 Proof of Theorem 2: feedback stability

At an interior three-population equilibrium, define

$$a = -F_x > 0, \quad b = F_y > 0, \quad c = F_q Q_z > 0,$$

$$d = -H_x > 0, \quad e = -H_y > 0, \quad f = P_x > 0, \quad g = P_y > 0, \quad h = -P_z > 0.$$

The Jacobian is

$$J_3 = \begin{pmatrix} -aX & bX & cX \\ -dY & -eY & 0 \\ fZ & gZ & -hZ \end{pmatrix}.$$

For the characteristic polynomial $r^3 + a_1 r^2 + a_2 r + a_3 = 0$, direct expansion gives

$$\begin{aligned} a_1 &= aX + eY + hZ, \\ a_2 &= XY(ae + bd) + XZ(ah - cf) + YZeh, \\ a_3 &= XYZ\{h(ae + bd) - c(ef - dg)\}. \end{aligned}$$

Because $a_1 > 0$, the Routh–Hurwitz conditions reduce to $a_2 > 0$, $a_3 > 0$, and $a_1 a_2 > a_3$. Since the first and third terms of a_2 are positive, $ah > cf$ is sufficient for $a_2 > 0$. If $ef > dg$, then $a_3 > 0$ is equivalent to

$$\frac{c(ef - dg)}{h(ae + bd)} < 1.$$

If $ef \le dg$, then $-c(ef - dg) \ge 0$, hence $a_3 > 0$ automatically.

2 Affine benchmark derivations

With

$$F = A + kz + \beta y - \gamma x, \qquad H = B - \delta x - \nu y,$$

the stationary conditions are

$$\gamma x - \beta y = A + kz, \qquad \delta x + \nu y = B.$$

Solving gives

$$x^* = \frac{\nu(A + kz) + \beta B}{\gamma\nu + \beta\delta}, \qquad y^* = \frac{\gamma B - \delta(A + kz)}{\gamma\nu + \beta\delta}.$$

The comparative statics follow immediately.

2.1 Boundary thresholds

On the upper commitment boundary $y = 1$, the focal stationary condition gives

$$x = \frac{A + kz + \beta}{\gamma}.$$

Commitment leaves $y = 1$ when $H(x, 1) = 0$, which yields

$$z_C = \frac{\gamma(B - \nu)/\delta - A - \beta}{k}.$$

On the lower boundary $y = 0$, $H(x, 0) = 0$ gives $x = B/\delta$. Substitution into the focal stationary condition yields

$$z_E = \frac{\gamma B/\delta - A}{k}.$$

For the one-population M1 benchmark $F = A + kz - \gamma x$, the upper search boundary $x = 1$ is reached at

$$z_H = \frac{\gamma - A}{k}.$$

2.2 Affine three-population stability term

For

$$P = G + \phi x - \omega(1 - y) - \xi z,$$

substitution into the general determinant term gives

$$a_3 = XYZ\{\xi(\gamma\nu + \beta\delta) - k(\nu\phi - \delta\omega)\}.$$

Thus the positive visibility–search–traffic loop dominates the determinant damping term when

$$k(\nu\phi - \delta\omega) \geq \xi(\gamma\nu + \beta\delta).$$

This condition is analytical; the simulations below only illustrate parameter regions around it.

3 Heterogeneity and role reversal

3.1 Heterogeneous susceptibility and targeted exposure

Under the multiplicative operator $\mathcal{U} = \kappa z s r$, let $\kappa_H > \kappa_L$ and let ρ denote the high-susceptibility population share. With group-specific effective exposure z_H, z_L, the aggregate first-order updating pressure is proportional to

$$K = \rho\kappa_H z_H + (1 - \rho)\kappa_L z_L.$$

Holding average exposure constant, concentrating exposure among high-susceptibility agents raises K. This is a direct implication of the updating operator and does not require an additional strategic payoff equation.

3.2 Role reversal

Let side A receive the initial visibility shock and side B respond. Write

$$\dot{x}_A = x_A(1 - x_A)F_A(Q_A(z), x_A, x_B), \qquad \dot{x}_B = x_B(1 - x_B)H_B(x_A, x_B).$$

If $(F_A)_q > 0$, $(F_A)_{x_A} < 0$, $(F_A)_{x_B} > 0$, $(H_B)_{x_A} < 0$, and $(H_B)_{x_B} < 0$, the proof of Theorem 1 applies without relabeling any sex or demographic group. Hence the mechanism is structurally bilateral rather than gender-specific.

4 Computational details

4.1 Baseline normalized parameters

The main text uses

$$A = .20, \quad \gamma = .80, \quad k = .80, \quad B = .75, \quad \delta = .90, \quad \nu = .25, \quad \beta = .10,$$

with $p_C = .65$ and $p_H(x) = .85 - .55x$. These values generate the threshold ordering $z_C \approx .181 < z_E \approx .583 < z_H = .750$.

4.2 Endogenous-visibility counterfactuals

The platform counterfactuals start from $(x_0, y_0, z_0) = (.25, .85, .99)$ with $G = .10$. The corrective scenario uses $(\phi, \omega, \xi) = (.35, .25, .80)$; the traffic-dominant scenario uses $(.60, .10, .60)$. Figures S1 and S2 show the corresponding paths.

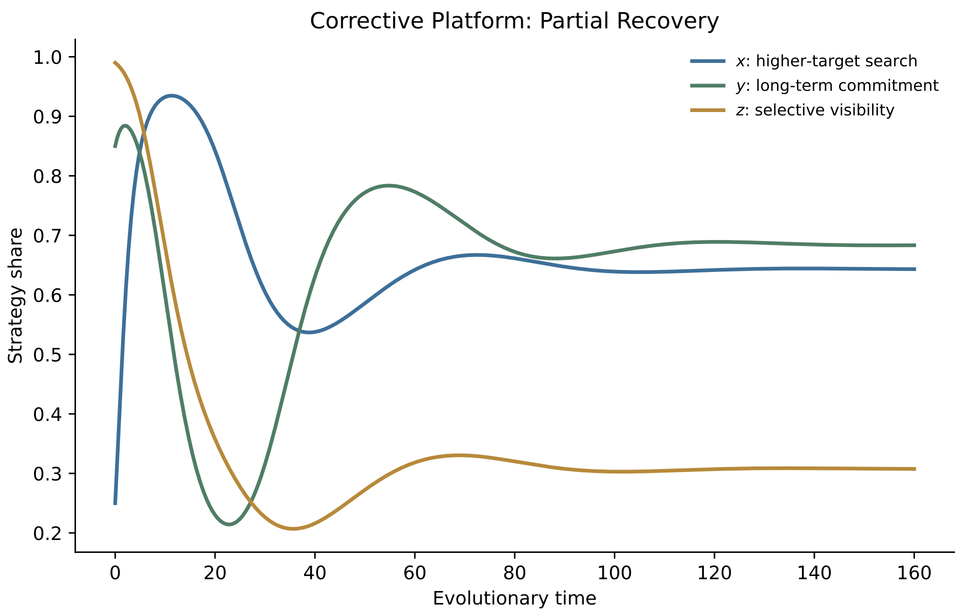

Figure S1: Corrective-platform counterfactual under the affine benchmark

4.3 Wide parameter envelope

The 10,000-draw scan uses the following ranges. Each draw is compared with its own no-visibility benchmark. The regime shares are 7.98% no mutual loss, 85.24% mutual loss with the platform not below its long-run benchmark, and 6.78% strict all-loss. These are parameter-space shares, not real-world probabilities.

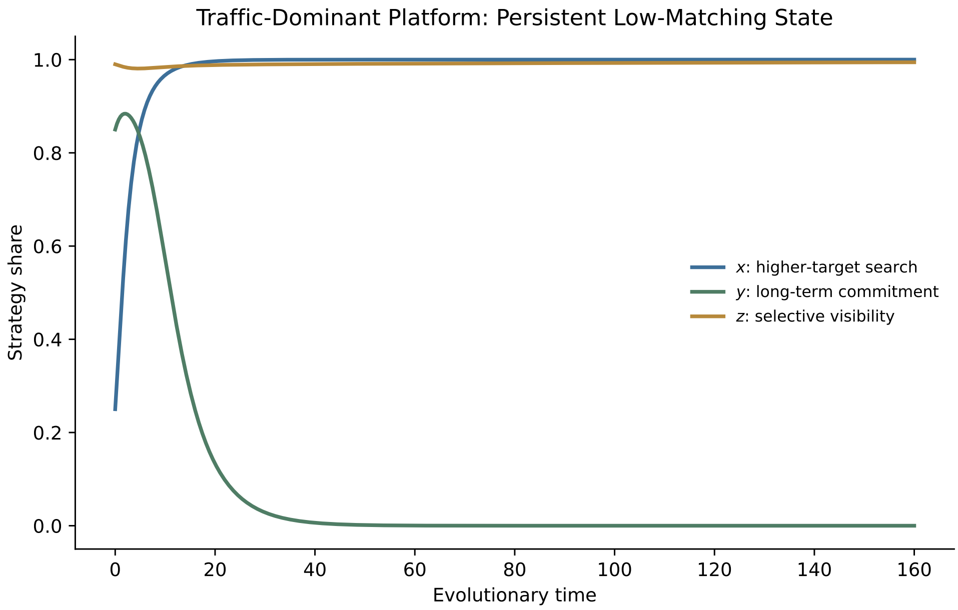

Figure S2: Traffic-dominant counterfactual under the affine benchmark

Parameter	Interpretation	Range
k	visibility-to-aspiration amplification	$[0.05, 1.20]$
γ	calibration/congestion	$[0.40, 2.00]$
δ	cross-side commitment response	$[0.05, 1.20]$
ϕ	traffic reward	$[0.05, 0.90]$
ω	ecosystem correction	$[0.05, 1.20]$
ξ	saturation/self-correction	$[0.30, 1.80]$

Table S1: Six-parameter robustness envelope

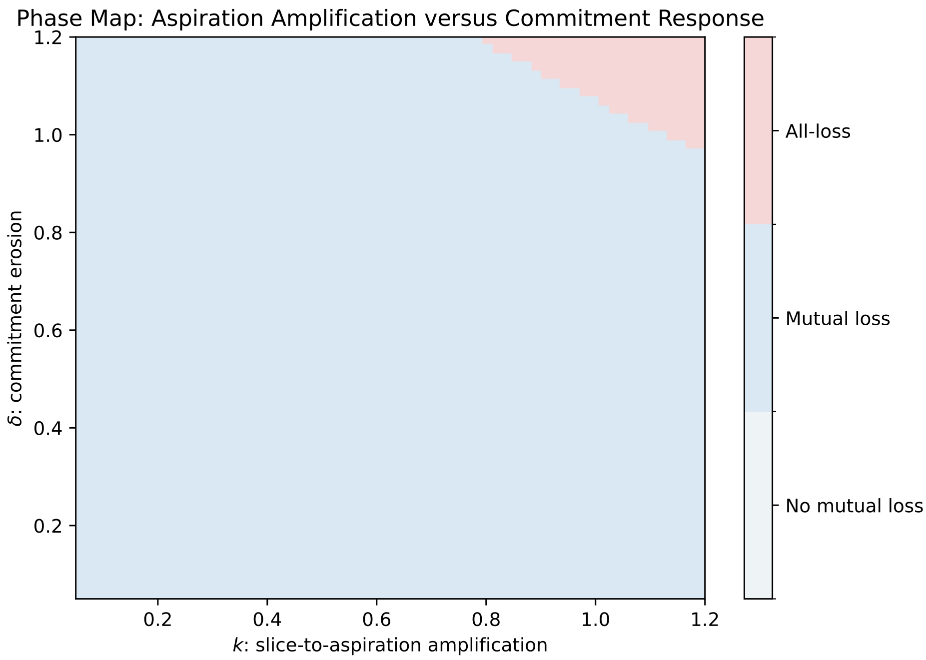

Figure S3: Supplementary regime map for visibility amplification and commitment response

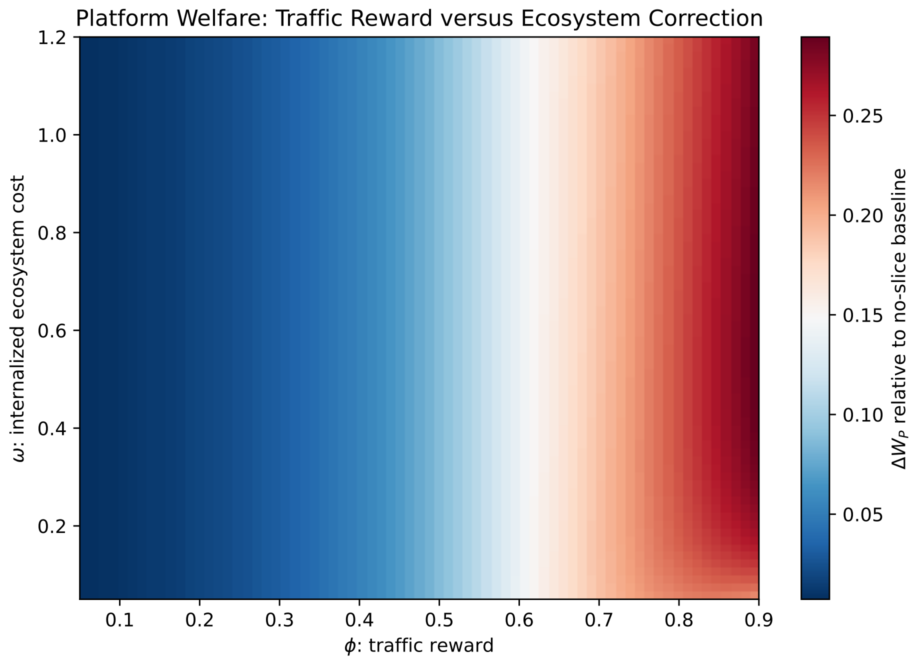

Figure S4: Supplementary platform-welfare map

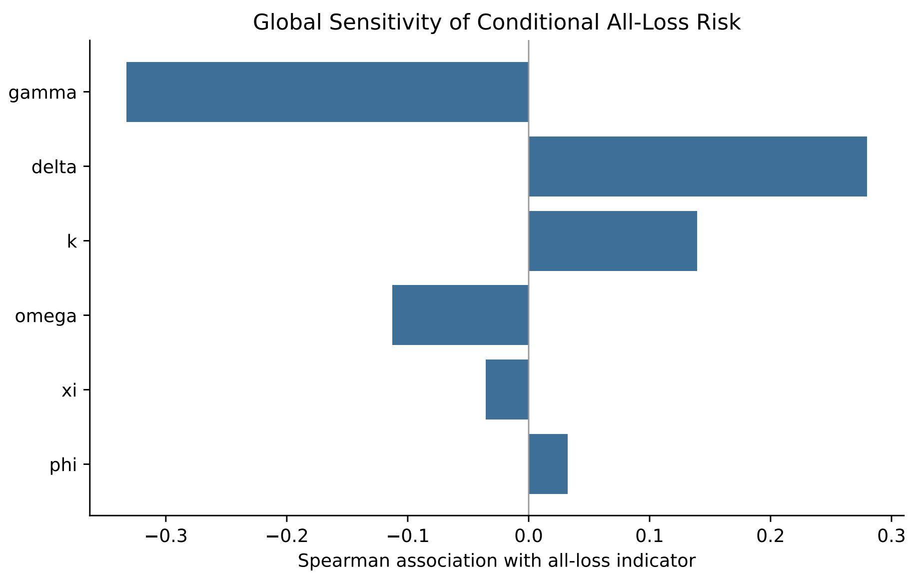

Figure S5: Global rank sensitivity of the conditional all-loss classification

4.4 Initial-condition and ecosystem-cost checks

The same structural parameter draws were evolved from $z_0 \in \{0.35, 0.60, 0.99\}$. For a fixed parameter vector, long-run outcomes were similar across these initial visibility states. The smooth baseline system therefore does not establish strong hysteresis.

The realized long-run ecosystem-cost weight Ω was varied from 0.2 to 1.2. The strict all-loss share rises from approximately 2.2% to 9.2%. This confirms that platform loss is conditional on the welfare normalization, whereas the analytical coordination result in the main text does not depend on Ω.

5 Reproducibility

The submission package contains the scripts used to reproduce the numerical trajectories, the 10,000-draw parameter scan, the phase maps, and the sensitivity summaries. All random draws use a fixed seed. The numerical exercises are mechanism illustrations rather than structural estimates.